Inorganic Chemistry

Article

pubs.acs.org/IC

Modulation of Energy Transfer into Sequential Electron Transfer upon Axial Coordination of Tetrathiafulvalene in an Aluminum(III) Porphyrin−Free-Base Porphyrin Dyad

Prashanth K. Poddutoori,*[,†] Lucas P. Bregles,[†] Gary N. Lim,[‡] Patricia Boland,[†] Russ G. Kerr,[†] and Francis D'Souza*[,‡]

[†]Department of Chemistry, University of Prince Edward Island, 550 University Avenue, Charlottetown, PE C1A 4P3, Canada

[‡]Department of Chemistry, University of North Texas, 1155 Union Circle, #305070, Denton, Texas 76203-5017, United States

Supporting Information

ABSTRACT: Axially assembled aluminum(III) porphyrin based dyads and triads have been constructed to investigate the factors that govern the energy and electron transfer processes in a perpendicular direction to the porphyrin plane. In the aluminum(III) porphyrin−free-base porphyrin (AlPor-Ph-H_2Por) dyad, the AlPor occupies the basal plane, while the free-base porphyrin (H_2Por) with electron withdrawing groups resides in the axial position through a benzoate spacer. The NMR, UV−visible absorption, and steady-state fluorescence studies confirm that the coordination of pyridine appended tetrathiafulvalene (TTF) derivative (TTF-py or TTF-Ph-py) to the dyad in noncoordinating solvents afford vertically arranged supramolecular self-assembled triads (TTF-py→AlPor-Ph-H_2Por and TTF-Ph-py→AlPor-Ph-H_2Por). Time-resolved studies revealed that the AlPor in dyad and triads undergoes photoinduced energy and/or electron transfer processes. Interestingly, the energy and electron donating/accepting nature of AlPor can be modulated by changing the solvent polarity or by stimulating a new competing process using a TTF molecule. In modest polar solvents (dichloromethane and *o*-dichlorobenzene), excitation of AlPor leads singlet−singlet energy transfer from the excited singlet state of AlPor (^{1}AlPor*) to H_2Por with a moderate rate constant (k_{EnT}) of 1.78×10^8 s^{-1}. In contrast, excitation of AlPor in the triad results in ultrafast electron transfer from TTF to ^{1}AlPor* with a rate constant (k_{ET}) of 8.33×10^9−1.25×10^{10} s^{-1}, which outcompetes the energy transfer from ^{1}AlPor* to H_2Por and yields the primary radical pair TTF$^{+\bullet}$-AlPor$^{-\bullet}$-H_2Por. A subsequent electron shift to H_2Por generates a spatially well-separated TTF$^{+\bullet}$-AlPor-H_2Por$^{-\bullet}$ radical pair.

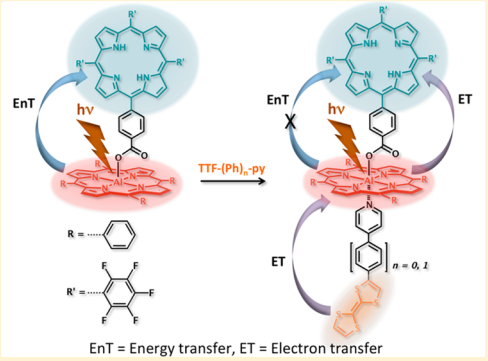

INTRODUCTION

Inspired by natural photosynthesis, many donor−acceptor (D−A) systems have been synthesized to mimic the function of light harvesting antenna[1−5] and reaction center[6−9] complexes. These studies aim not only at a better understanding of the photoinduced energy transfer (EnT) and electron transfer (ET) processes but also at building artificial photosynthetic systems for solar energy conversion and storage applications as well as photo- and electronic devices.[10−21] In most of these artificial systems, porphyrin (Por) has emerged as a promising building block and an attractive chromophore because they have structural similarities with chlorophyll as they absorb strongly in the visible region, are often highly fluorescent, and have rich redox chemistry, and most importantly, their optical and redox properties are easily tunable.[22] In combination with other photo and redox active species, porphyrins have been used to produce a wide array of covalent and noncovalent multicomponent systems to mimic the light harvesting and reaction center complexes of photosynthetic systems.[6,8,17,23−28] However, most of these model compounds deal with the photoinduced processes along the porphyrin plane. Little is known about these processes in the perpendicular (axial) direction to the porphyrin plane.[26,29−41] One reason for this is the difficulty associated with attaching different ligands to the porphyrin in the axial position. In this respect, aluminum(III) porphyrins (AlPors) are unique as they form (i) covalent bonds with carboxylic acids[42−49] or alcohols[50−53] and (ii) coordination bonds with Lewis bases[42,44,45,54,55] (e.g., pyridine or imidazole). Since AlPor can form two different types of axial bonds, it is possible to attach two different molecular components to the opposite faces. These advantages of AlPor provide an excellent opportunity to study the influence of electronic coupling, orientation, and reorganization energy on the energy and electron transfer processes in the perpendicular direction to the porphyrin plane.[42−45,56,57] Moreover, this particular geometry not only keeps the axial components spatially well separated from each other but also prevents aggregation between the molecules, which is a most common problem in porphyrin based D−A systems.

Received: May 26, 2015
Published: August 13, 2015

DOI: 10.1021/acs.inorgchem.5b01190
Inorg. Chem. 2015, 54, 8482−8494

Chart 1. Structures of the Investigated Compounds in This Study

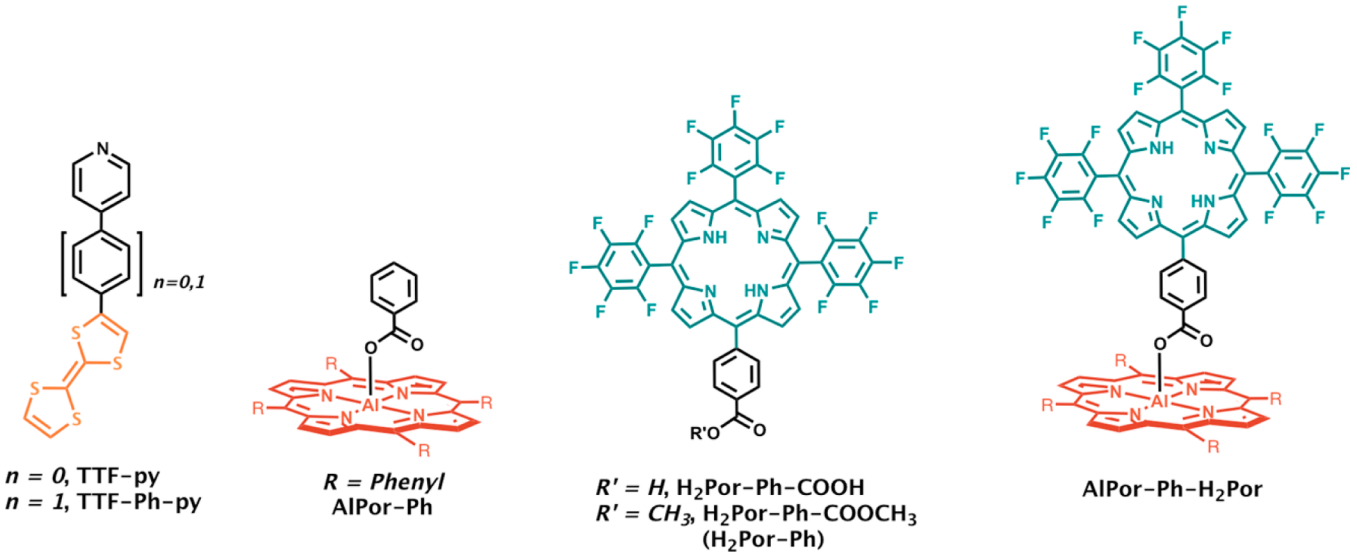

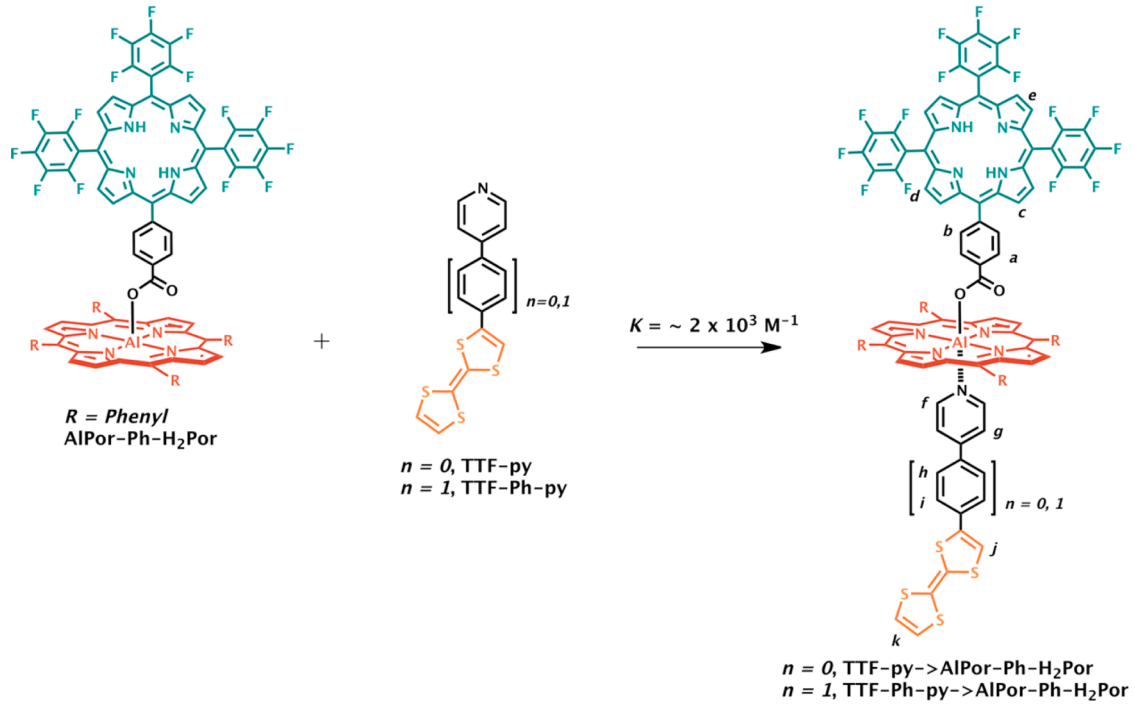

Figure 1. Formation of vertically arranged self-assembled supramolecular triads through Lewis acid–base interactions.

In a photosystem, the light harvesting antenna and the reaction center complex work together to perform the conversion of solar energy into chemical energy.[58−62] One of the similarities between the light harvesting antenna and reaction center complex is that they both utilize a chlorophyll molecule as the chromophore. However, chlorophyll's role is entirely different as it serves as an energy donor in the light harvesting antenna complex, whereas in the reaction center complex the "chlorophyll special pair" performs predominantly the role of an electron donor. This is because the surrounding protein alters the chlorophyll's spectral and redox properties for a desired role in each of these complexes.[63,64] For artificial systems, there is no surrounding protein, and therefore, other ways of tuning the spectral and redox potential of the photosensitizer must be required. To mimic the role of the chlorophyll in photosynthesis, here we report a new vertical AlPor based dyad aluminum(III) porphyrin–free-base porphyrin (AlPor-Ph-H_2Por, see Chart 1) and corresponding two axially arranged self-assembled triads tetrathiafulvalene–aluminum(III) porphyrin–free-base porphyrin (TTF-py→AlPor-Ph-H_2Por and TTF-Ph-py→AlPor-Ph-H_2Por, Figure 1). We have chosen tetrathiafulvalene (TTF) as the secondary donor because of its strong electron donating ability, which makes it an excellent candidate as a reductive electron quencher in D–A systems.[25,65,66] As an acceptor, we have selected free-base porphyrin (H_2Por) with electron withdrawing fluorinated phenyl substituents in its meso positions. Its positive redox potentials and strong spectral overlap with AlPor makes the selected H_2Por as an acceptor for both energy and electron transfer processes.[67,68] Time-resolved studies have shown that

DOI: 10.1021/acs.inorgchem.5b01190
Inorg. Chem. 2015, 54, 8482−8494

these compounds undergo photoinduced energy and/or electron transfer processes. We will also show that the energy and electron donating nature of AlPor can be modulated by changing the solvent polarity or by stimulating a new competing process using the TTF molecule. In the AlPor-Ph-H_2Por dyad, AlPor serves as an energy donor to the H_2Por. In contrast, the same AlPor in the triad acts as an electron acceptor/donor in the presence of a secondary electron donor TTF moiety.

EXPERIMENTAL SECTION

Synthesis. All chemicals and solvents used in this study were purchased from either Sigma-Aldrich Chemical Co. or Alfa-Asear. The synthesis of 5,10,15,20-tetra(phenyl)-porphyrinatoaluminum(III)-hydroxide (AlPor-OH), reference compound AlPor-Ph, and the pyridine appended tetrathiafulvalene derivatives (TTF-py and TTF-Ph-py) have been previously reported.[43,45] ***Caution:!*** *$AlMe_3$ reacts violently with water and therefore should be handled with great care. The reaction must be performed in anhydrous conditions.* The synthesis details of precursor porphyrins, 5-(4-methylcarboxyphenyl)-10,15,20-tri-(pentafluorophenyl)porphyrin (H_2Por-Ph−$COOCH_3$, from now on referred to as H_2Por-Ph) and 5-(4-carboxyphenyl)-10,15,20-tri-(pentafluorophenyl)porphyrin (H_2Por-Ph-COOH), are given in Supporting Information.

Preparation of AlPor-Ph-H_2Por. AlPor-OH (50 mg, 0.076 mmol) and H_2Por-Ph-COOH (71 mg, 0.077 mmol) were dissolved in 15 mL of dry dichloromethane. Anhydrous Na_2SO_4 (100 mg, 0.70 mmol) was added, and the resulting solution was stirred at room temperature under nitrogen atmosphere. After 12 h, the solution was passed through Na_2SO_4, and the solvent was removed under reduced pressure. The obtained product was washed with hexane to get the pure dyad as a purple solid. Yield: 110 mg (92%). Mass (ESI): m/z 1567.3076 $[M + H]^+$, calculated 1567.3085 for $C_{89}H_{43}AlF_{15}O_2N_8$. ^{1}H NMR (300 MHz, $CDCl_3$): ppm 9.16 (s, 8H), 8.83 (s, 4H), 8.59 (d, 2H, J = 4.8 Hz), 8.36 (d, 2H, J = 4.8 Hz), 8.25 (d, 8H, J = 6.0 Hz), 7.76 (m, 12H), 7.29 (d, 2H, J = 8.0 Hz), 5.51 (d, 2H, J = 8.0 Hz), −3.05 (bs, 2H).

Physical Methods. *NMR Spectroscopy and Mass Spectrometry.* ^{1}H NMR and ^{1}H−^{1}H COSY spectra were recorded with a Bruker Avance 300 MHz NMR spectrometer using $CDCl_3$ as the solvent. High-resolution mass spectrometry analysis was performed on an LTQ Orbitrap Velos mass spectrometer (ThermoScientific) using an ESI ion source operating in positive mode with a resolution of 30,000, monitoring a mass range from 150 to 2000 atomic mass units (amu).

Voltammetry. Cyclic voltammetric experiments (in dichloromethane with 0.1 M tetrabutylammonium perchlorate ($TBAClO_4$)) were performed on the Potentiostat/Galvanostat Model 283 (EG & G Instruments, Princeton Applied Research) electrochemical analyzer (working electrode, platinum; auxiliary electrodes, Pt wire; reference electrode, Ag/AgCl). The Fc^+/Fc (Fc = ferrocene, $E_{1/2}(Fc^+/Fc)$ = 0.48 V vs SCE in CH_2Cl_2, 0.1 M $TBAClO_4$ under our experimental conditions) redox couple was used to calibrate the potentials, which were reported in V vs SCE. Spectroelectrochemical study was performed by using a cell assembly (SEC-C) supplied by ALS Co., Ltd. (Tokyo, Japan). This assembly comprises a Pt counter electrode, a 6 mm Pt Gauze working electrode, and an Ag/AgCl reference electrode in a 1.0 mm path length quartz cell. The optical transmission was limited to 6 mm covering the Pt Gauze working electrode.

Steady-State UV−Visible Absorption and Emission Spectroscopy. The UV/vis spectra were recorded with a Varian Cary 50 Bio UV−vis spectrometer. Concentration of the samples used for these measurements ranged from 1×10^{-6} M (porphyrin Soret band) to 5×10^{-5} M (Q-bands) solutions. Steady-state fluorescence spectra were recorded using a Photon Technologies International LS-100 luminescence spectrometer (L-format), equipped with a 70 W xenon lamp, running with Felix software.

Absorption and Fluorescence Titrations. Absorption titrations were carried out in dry dichloromethane at concentration of 6×10^{-5} M appropriate for measuring the porphyrin Q bands. A solution containing the acceptor (A = AlPor-Ph-H_2Por or AlPor-Ph) was placed in a cuvette and titrated by adding aliquots of a concentrated solution of the donor (D = TTF-py, TTF-Ph-py, or py). The donor solution also contained the acceptor at its initial concentration so that the porphyrin concentration remained constant throughout the titration. The binding constants were calculated using the Benesi−Hildebrand equation,[69] $[A]/Abs = (1/[D])(1/\varepsilon K) + (1/\varepsilon)$, where, [A] is the total concentration of bound and unbound acceptor and is kept fixed, Abs is the absorption of the complex at the wavelength λ, [D] is the total concentration of the donor which is varied, K is the binding constant, and ε is the molar absorptivity of the D−A complex. In an analogous manner, steady-state fluorescence titrations were carried out in dry dichloromethane using solutions at a constant concentration of A and varying concentrations of D. The solutions were excited at the isosbestic point wavelength, which was obtained from the corresponding absorption titrations.

Time-Resolved Fluorescence Spectroscopy. A time-correlated single-photon-counting apparatus utilizing a picosecond-pulsed diode laser was used to measure the porphyrin fluorescence decay. Excitation pulses were delivered at 406 nm by a picosecond diode laser (PicoQuant, PDL 800-B), 54 ps fwhm, at a repetition rate of 10 MHz. The porphyrin fluorescence was measured by a Hamamatsu R3809 microchannel plate photomultiplier screened by a double monochromator. A single-photon-counting PC card (Becker & Hickl, SPC-730) was used for data collection. The instrument response time of the system was 80 ps.

Femtosecond Laser Flash Photolysis. Femtosecond transient absorption spectroscopy experiments were performed using an Ultrafast Femtosecond Laser Source (Libra) by Coherent incorporating a diode-pumped, mode locked Ti:sapphire laser (Vitesse) and a diode-pumped intracavity doubled Nd:YLF laser (evolution) to generate a compressed laser output of 1.45 W. For optical detection, a Helios transient absorption spectrometer coupled with a femtosecond harmonics generator, both provided by Ultrafast Systems LLC, was used. The source for the pump and probe pulses were derived from the fundamental output of Libra (compressed output 1.45 W, pulse width 100 fs) at a repetition rate of 1 kHz. Ninety-five percent of the fundamental output of the laser was introduced into a harmonic generator that produces second and third harmonics of 400 and 267 nm besides the fundamental 800 nm for excitation, while the rest of the output was used for the generation of a white light continuum. In the present study, the second harmonic 400 nm excitation pump was used in all of the experiments. The absorbance of AlPor and H_2Por are in ∼1:2 ratio at this excitation wavelength. Kinetic traces at appropriate wavelengths were assembled from the time-resolved spectral data. Data analysis was performed using Surface Xplorer software supplied by Ultrafast Systems. All measurements were conducted in degassed solutions at 298 K.

RESULTS AND DISCUSSION

Synthesis. A porphyrin dyad was prepared by previously established methods[42,44,45,70] in quantitative yields. Complete experimental details are shown in Schemes S1 and S2 (see Supporting Information) as well as in the Experimental Section. The dyad (AlPor-Ph-H_2Por) was prepared by reacting equal molar ratios of AlPor-OH and H_2Por-Ph-COOH, and the reaction was monitored by NMR spectroscopy. The obtained dyad was stored on a freshly prepared $CaCl_2$ desiccator prior to optical studies. The triads shown in Figure 1 were assembled by using the dyad (AlPor-Ph-H_2Por) and TTF-py/TTF-Ph-py derivatives in noncoordinating solvents. Lewis acid−base interactions were utilized to build these vertically arranged supramolecular self-assembled triads. NMR, UV−visible absorption, and steady-state fluorescence titrations were employed to monitor the formation of triads. However, the formed self-assembled triads could not be isolated.

DOI: 10.1021/acs.inorgchem.5b01190
Inorg. Chem. 2015, 54, 8482−8494

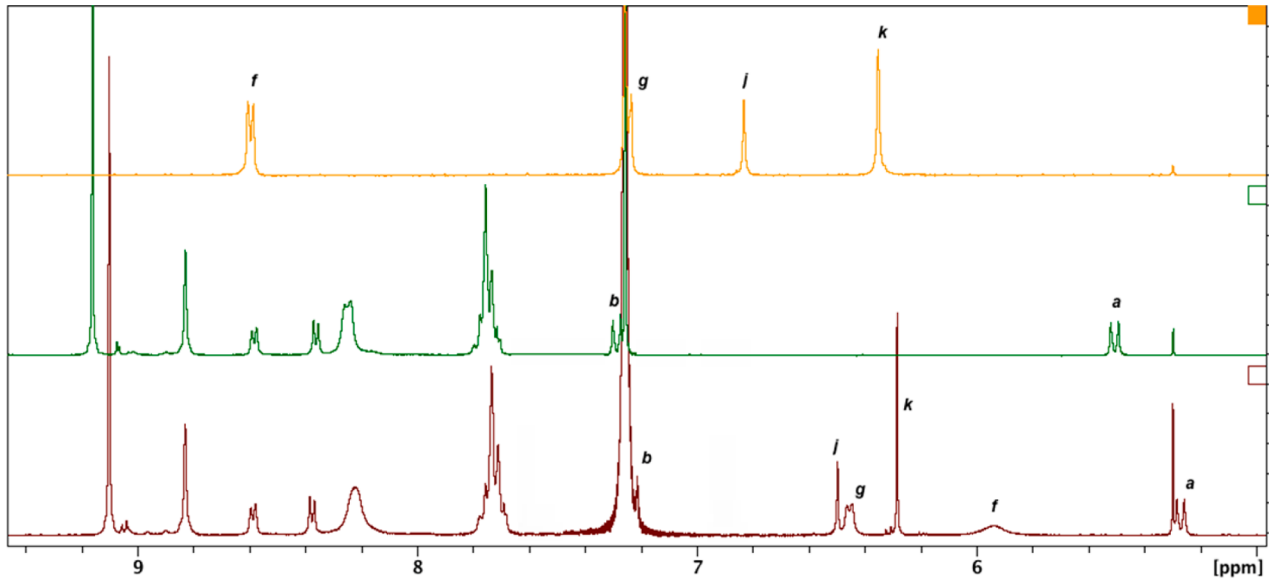

Figure 2. ^{1}H NMR (300 MHz) spectra of TTF-py (top), AlPor-Ph-H_2Por (middle), and TTF-py→AlPor-Ph-H_2Por (bottom) in $CDCl_3$.

Structural Characterization. Preliminary characterization of the dyad was carried out by ESI mass spectrometry. The mass spectrum of the dyad AlPor-Ph-H_2Por showed peaks at 1567 and 639, which corresponds to the mass (m/z) of $[M + H]^+$ and $[M - \text{axial } H_2\text{Por}]^+$, respectively. The ^{1}H NMR spectra of the dyad AlPor-Ph-H_2Por and one of its monomers from which it was prepared, H_2Por-Ph-COOH, are shown in Figure S4. Shielding effects are apparent for the protons on the axial porphyrin subunit. For example, resonances due to the phenyl protons *b* and *a* (Figure 1), which appear at 8.58 and 8.37 ppm in the isolated H_2Por-Ph-COOH porphyrin, are strongly shifted upfield to 7.29 and 5.51 ppm, respectively in the dyad AlPor-Ph-H_2Por due to the ring current effect of the porphyrin macrocycle. Similarly, resonances due to the β-protons (*c*, *d*, and *e*) as well as inner NH protons are shifted upfield compared to the corresponding resonances in the spectrum of compound H_2Por-Ph-COOH. These chemical shifts (δ) agree well with those of the axial bonding type porphyrin systems.[42,44,45,70] Hence, the $\Delta\delta$ values (i.e., $\delta_{\text{monomer}} - \delta_{\text{dyad}}$) are a function of their proximity to the porphyrin ring.

Figure 2 shows the ^{1}H NMR spectrum of the triad (TTF-py→AlPor-Ph-H_2Por (bottom), that is, a 1:1 mixture of AlPor-Ph-H_2Por and TTF-py) along with the individual spectra of AlPor-Ph-H_2Por (middle) and TTF-py (top). In the triad complex, TTF-py→AlPor-Ph-H_2Por, shielding due to the porphyrin ring causes an upfield shift of the TTF-py protons on the pyridine unit (*f* and *g*) and the TTF moiety (*j* and *k*). The magnitude of the shift depends on the distance of the protons from the porphyrin ring; hence, the pyridinyl protons (*f* and *g*) display a large shift indicating that coordination occurs via the pyridinyl group. On the benzoate bridging group to the H_2Por, the protons (*a*) closest to the porphyrin ring show an increased upfield shift upon coordination, suggesting that the aluminum(III) center lies out of the porphyrin plane in AlPor-Ph-H_2Por and is pulled into the plane when TTF-py coordinates. Analogous results were obtained from the triad, TTF-Ph-py→AlPor-Ph-H_2Por (Figures S5).

UV−Visible Absorption Spectroscopy. The UV−visible spectra of the dyad AlPor-Ph-H_2Por and its reference compounds (AlPor-Ph and H_2Por-Ph) were measured in dichloromethane, and the spectra are shown in Figure 3. The band positions (Q-bands and B- or Soret bands) and their molar extinction coefficients are summarized in Table 1. As shown in Figure 3 and Table 1, the absorption spectrum of the dyad is essentially a linear combination of its reference porphyrins. Furthermore, the band positions and molar extinction coefficients (ε) of the dyad are similar to corresponding monomer porphyrins. Therefore, the majority of the absorbance at 510, 547, and 639 nm is attributed to the H_2Por (87%), AlPor (90%), and H_2Por (60%), respectively. The absorption spectrum of the dyad AlPor-Ph-H_2Por, also measured in acetonitrile, is shown in Figure S6. Noticeable differences are observed when compared with the spectrum in dichloromethane. The AlPor bands are red-shifted (~10 nm) due to the coordination of the solvent at the Al center of the AlPor. However, the band positions and molar extinction coefficients remain similar to its monomeric compounds. Overall, the absorption studies suggest that there exist no or weak interactions between basal porphyrin (AlPor) and axial porphyrin (H_2Por). The absorption bands of AlPor and H_2Por

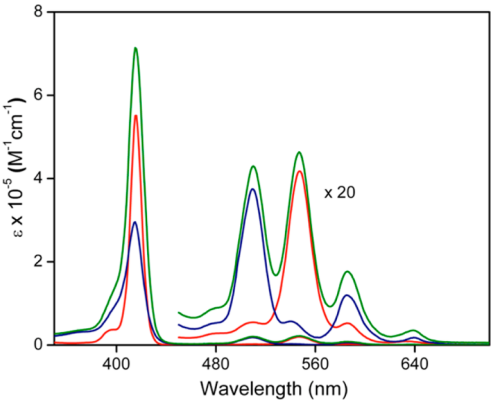

Figure 3. UV−visible absorption spectra of dyad AlPor-Ph-H_2Por (green) and reference compounds H_2Por-Ph (blue) and AlPor-Ph (red) in dichloromethane.

DOI: 10.1021/acs.inorgchem.5b01190
Inorg. Chem. 2015, 54, 8482−8494

Table 1. UV−Visible Absorption and Steady-State Fluorescence Data of Investigated Compounds

	absorption[a] λ_{max} (nm) (log ε)		fluorescence			
			dichloromethane λ_{em} (nm) (%Q)		acetonitrile λ_{em} (nm) (%Q)	
sample	Q-bands/TTF	B-band	λ_{ex} = 550 nm	λ_{ex} = 640 nm	λ_{ex} = 560 nm	λ_{ex} = 640 nm
AlPor-Ph	585 (3.42), 547 (4.32), 510 (3.44)	416 (5.74)	595, 646		608, 662	
H_2Por-Ph	639 (2.96), 585 (3.78), 540 (3.46), 510 (4.27)	415 (5.47)	642, 708	708	640, 704	704
AlPor-Ph-H_2Por	639 (3.25), 586 (3.95), 547 (4.37), 510 (4.33)	415 (5.85)	596, 642, 708 (90%)	706	608, 660, 704 (91%)	706 (56%)
TTF-py	435 (3.45), 324 (4.17), 285 (4.22)					
TTF-Ph-py	428 (3.64), 298 (4.48)					

[a]Spectra were measured in dichloromethane.

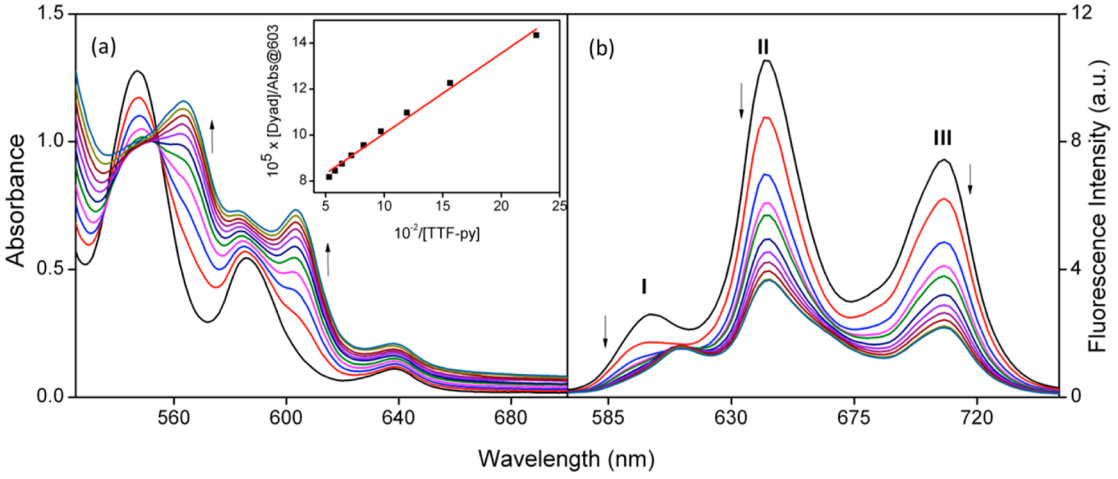

Figure 4. (a) Absorption and (b) fluorescence titrations of AlPor-Ph-H_2Por with TTF-py in dichloromethane. The inset shows the Benesi−Hildebrand plot of the change of absorbance at 603 nm. TTF-py was added up to 1.88×10^{-3} M in 20 μL (2.22×10^{-4} M) increments to 1 mL (6×10^{-5} M) solution of AlPor-Ph-H_2Por. The excitation wavelength was chosen at the isosbestic point, 555 nm, which was obtained from absorption titrations.

are weakly overlapping; therefore, by choosing the wavelengths of 550/560 and 640 nm it is possible to excite mostly AlPor and the axial H_2Por units, respectively, for steady-state fluorescence studies. The py-appended TTF derivatives (TTF-py and TTF-Ph-py) have relatively weak and very broad absorption bands (see Figure S7) at λ = 304 (average of 285 and 324 nm bands) and λ = 435 nm for TTF-py, and at λ = 298 and 428 nm for TTF-Ph-py.

Figure 4a shows absorption titrations of TTF-py vs AlPor-Ph-H_2Por in dichloromethane. Upon addition of TTF-py, the Q bands of the porphyrin 547 and 586 nm are shifted to 563 and 603 nm. An isosbestic point is observed at 555 nm, indicating the formation of TTF-py→AlPor-Ph-H_2Por in equilibrium, and the shifts in the porphyrin bands are typical of axial coordination of nitrogen ligands to AlPors.[42,44,45,54,55] Benesi−Hildebrand analysis[69] (Figure 4A, inset) gives a linear plot indicating that a 1:1 complex is formed, and the slope yields a binding constant $K = 1.8 \times 10^3$ M^{-1}. In a similar fashion, the binding constant K was calculated for the titrations of TTF-Ph-py vs AlPor-Ph-H_2Por (Figure S8a), py vs AlPor-Ph-H_2Por (Figure S10a), and the data are summarized in Table S1. Titrations TTF-py vs AlPor-Ph and TTF-Ph-py vs AlPor-Ph and corresponding binding constants have been reported previously.[45] Titrations of TTF-py/TTF-Ph-py with AlPor-Ph-H_2Por have shown greater binding ($\sim 2.0 \times 10^3$ M^{-1}) than that of the AlPor-Ph ($\sim 1.0 \times 10^3$ M^{-1}), which suggests that as the electron withdrawing nature (Ph < H_2Por) of the axial ligand increases, the Al center becomes a better Lewis acid; hence, it binds stronger with the Lewis base pyridine. Together with NMR and absorption titrations, we conclude the formation of the triad (TTF-py→AlPor-Ph-H_2Por or TTF-Ph-py→AlPor-Ph-H_2Por) in the solution.

Cyclic Voltammetry. Cyclic voltammetry of the newly investigated dyad and reference monomers were measured in 0.1 M $TBAClO_4$ dichloromethane with ferrocene as an internal standard. Representative voltammograms are shown in Figure S11, and the data are summarized in Table 2. The redox processes of all of the compounds are found to be one-electron reversible based on the peak-to-peak separation values, and the cathodic-to-anodic peak current ratio. The voltammogram of the dyad is essentially a sum of the voltammograms of its reference monomers AlPor-Ph and H_2Por-Ph. During the cathodic scan, the dyad showed three reduction processes. On the basis of the respective monomers, the observed first and third processes are assigned to the first and second reduction of

Table 2. Redox Potential Data of Investigated Compounds in Dichloromethane with 0.1 M $TBAClO_4$ as a Supporting Electrolyte

	potential (V vs SCE)	
sample	oxidation	reduction
AlPor-Ph-H_2Por	0.91, 1.12, 1.54, 1.70	−0.87, −1.20, −1.35
AlPor-Ph	0.91	−1.21
H_2Por-Ph	1.51, 1.77	−0.87, −1.30
TTF-py	0.48, 0.83	
TTF-Ph-py	0.47. 0.87	

DOI: 10.1021/acs.inorgchem.5b01190
Inorg. Chem. 2015, 54, 8482−8494

the axial porphyrin (H_2Por) unit, whereas the second process is assigned to the first reduction of the AlPor unit. Conversely, the anodic scan reveals four oxidation processes for the dyad. The first two processes are assigned to the AlPor, and later processes belong to the axial H_2Por unit. As anticipated, the dyad showed a combination of processes from their respective monomeric porphyrin units without any perturbation in their redox potentials. Therefore, the observed cyclic voltammograms and redox data suggest that the components of the dyad do not influence one another significantly. The TTF derivatives (TTF-py and TTF-Ph-py) show two processes corresponding to the first and second oxidations of the TTF moiety. These results have been published elsewhere.[45]

The redox potentials are used in combination with optical data to estimate the energetics of the energy and electron transfer reactions in the investigated compounds. Figure 5

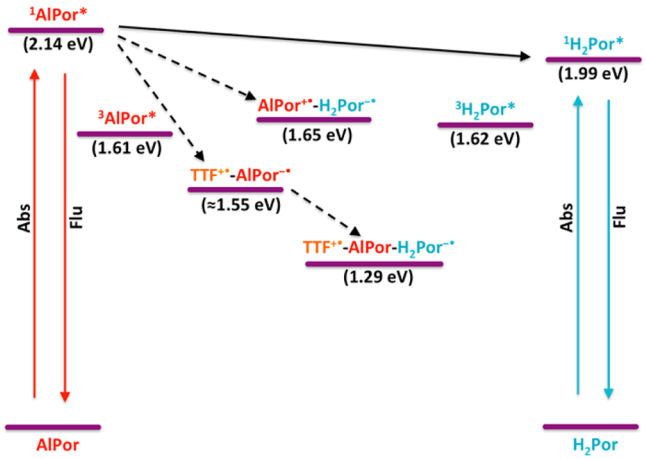

Figure 5. Energy level diagram for the dyad and its corresponding self-assembled triads in dichloromethane. Black solid and dashed lines represent energy transfer and electron transfer, respectively.

summarizes the energy levels of the dyad and its corresponding supramolecular triads. The energies of the radical ion pair states (E_{CS}) and free energy change for the charge separation (ΔG_{CS}) are estimated using the Weller equation:[71,72]

$$E_{CS} = e[E_{1/2}(D^{•+}/D) - E_{1/2}(A/A^{•-})] + G_S \quad (1)$$

$$\Delta G_{CS} = E_{CS} - E_{0-0} \quad (2)$$

where $E_{1/2}(D^{•+}/D)$ is the first oxidation potential of the donor, $E_{1/2}(A/A^{•-})$ is the first reduction potential of the acceptor. G_S is ion-pair stabilization and incorporates both the solvent-dependent Coulomb energy change upon ion-pair formation and the free energy of solvation of the ions,

$$G_S = \frac{e^2}{4\pi\varepsilon_0}\left[\left(\frac{1}{2R_+} + \frac{1}{2R_-} - \frac{1}{R_{D-A}}\right)\frac{1}{\varepsilon_S} - \left(\frac{1}{2R_+} + \frac{1}{2R_-}\right)\frac{1}{\varepsilon_R}\right] \quad (3)$$

where R_+, R_-, and $R_{D\text{-}A}$ are the donor radius, acceptor radius, and center-to-center distance between the donor and acceptor, respectively.[73] ε_S is the dielectric constant of the solvent used for the photophysical studies (9.1 and 37.5 for dichloromethane and acetonitrile, respectively). ε_R is the dielectric constant of the solvent used for measuring the redox potentials, in this case dichloromethane. The lowest excited singlet state energy (E_{0-0}) is estimated from the crossing point of absorption and fluorescence spectra and found to be 579 and 620 nm for AlPor and H_2Por, respectively (see Figure S12). Similarly, the band position of the phosphorescence spectrum (see Figure S13) at 768 and 770 nm of AlPor-Ph and H_2Por-Ph, respectively, is taken as the lowest excited triplet state. The calculated energy levels suggest that energy transfer (EnT), electron transfer (ET), and electron shift (ES) processes are energetically feasible in the investigated dyad and its corresponding self-assembled supramolecular triads. With acetonitrile as the solvent, the radical ion-pairs are found to be slightly lower in energy than in dichloromethane (Figure S14).

Fluorescence Spectroscopy. Steady-state fluorescence measurements were performed in dichloromethane and acetonitrile. Figure 6a illustrates the fluorescence spectra of the dyad and its corresponding monomers in dichloromethane, and the data are summarized in Table 1. As shown in Figure 6a, excitation of the dyad at 550 nm (where 90% of light is absorbed by AlPor) results in the appearance of fluorescence bands due to H_2Por (bands II and III) and AlPor (bands I and II) components. It was found that the fluorescence band maxima of AlPor and H_2Por components are quite close to those of AlPor-Ph or H_2Por-Ph, respectively. However, the fluorescence intensity of the AlPor component is strongly quenched (90%, emission monitored at the band I; see Table 1) in comparison with that of the reference compound AlPor-

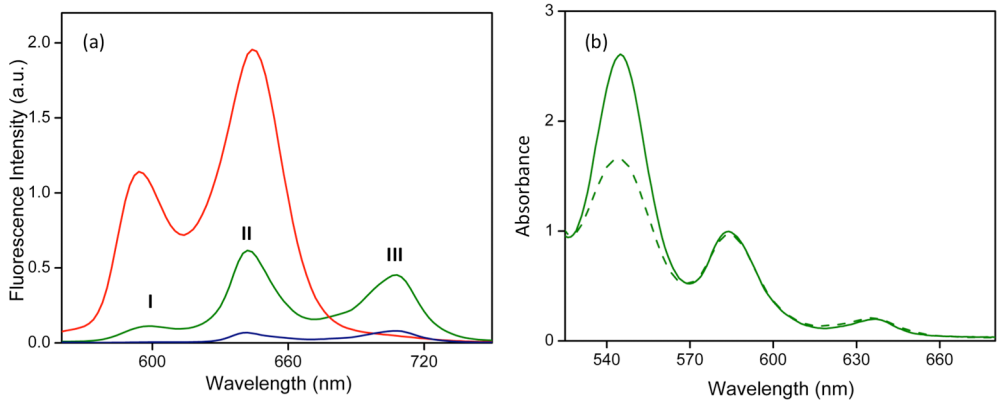

Figure 6. (a) Steady-state fluorescence spectra of AlPor-Ph-H_2Por (green), AlPor-Ph (red), and H_2Por-Ph (blue) with excitation at 550 nm in dichloromethane. (b) Absorption (solid) and corrected fluorescence excitation (dashed) spectra of the dyad in dichloromethane. The spectra were normalized between 610 and 650 nm. The excitation spectrum was collected at 720 nm corresponding to the emission of H_2Por.

DOI: 10.1021/acs.inorgchem.5b01190
Inorg. Chem. 2015, 54, 8482−8494

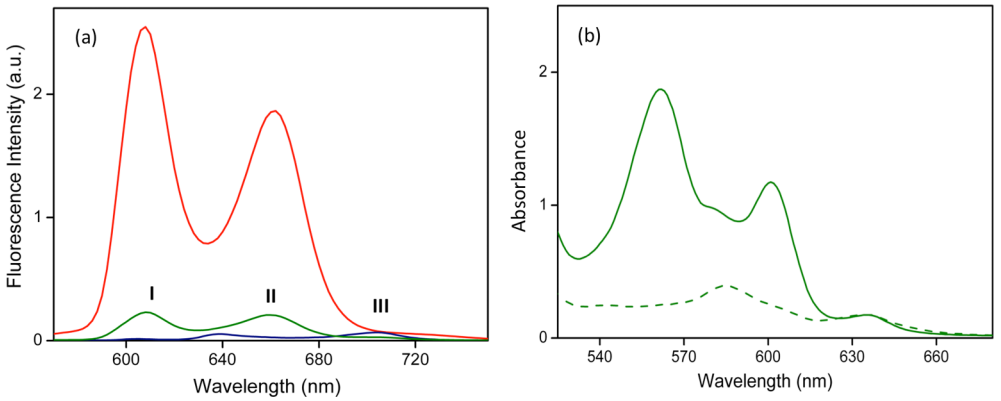

Figure 7. (a) Steady-state fluorescence spectra of AlPor-Ph-H_2Por (green), AlPor-Ph (red), and H_2Por-Ph (blue) with excitation at 560 nm in acetonitrile. (b) Absorption (solid) and corrected fluorescence excitation (dashed) spectra of the dyad in acetonitrile, and the spectra were normalized between 610 and 650 nm. The excitation spectrum was collected at 720 nm corresponding to the emission of H_2Por.

Ph. In contrast, band III intensity increased with respect to H_2Por-Ph. These results clearly suggest that the AlPor first excited singlet state (^{1}AlPor*) is being strongly quenched by H_2Por through the singlet−singlet energy transfer mechanism. The possibility of energy transfer is supported by significant spectral overlap between the fluorescence spectrum of AlPor and absorption spectrum of H_2Por (Figure S15a). This is further investigated by using the fluorescence excitation spectrum. Figure 6b shows the corrected excitation spectrum of the dyad in dichloromethane collected at 720 nm (emission monochromator) where only the H_2Por emits. Overlap of the corrected and normalized excitation spectra with the corresponding absorption spectra revealed that the singlet−singlet energy transfer (EnT) efficiency is ∼70% for the dyad in dichloromethane. Thus, it appears that the major portion (70% out of 90%) of ^{1}AlPor* state is quenched due to the energy transfer process. The remaining 20% quenching could be attributed to the electron transfer (ET) from ^{1}AlPor* to H_2Por as the Gibbs free energy change (ΔG_{CS}) for this process was found to be exergonic (−0.49 eV) in dichloromethane. Furthermore, excitation of the dyad at 640 nm (where 60% of light is absorbed by H_2Por) showed a band exclusively due to the free-base component in the ∼720 nm (band III) region, and its intensity was found to be similar to the sum of the calculated spectrum of H_2Por-Ph + AlPor-Ph (Figure S15b). Thus, we conclude that electron transfer from AlPor to the excited singlet state of free-base porphyrin ($^1H_2$Por*) is weak or negligible, although the corresponding ΔG_{CS} is estimated to be −0.34 eV.

To investigate the quenching processes in high polar solvents, fluorescence was measured in acetonitrile. Figure 7a illustrates the fluorescence spectra of the dyad and corresponding monomers in acetonitrile. Solutions were excited at 560 nm, where AlPor absorbs 95% of light. The band positions of the dyad are quite similar to its reference monomeric porphyrins (Figure 7a). However, two changes can be seen: (1) fluorescence bands of AlPor are red-shifted (∼10 nm) in comparison with dichloromethane data, and (2) fluorescence intensity is strongly quenched (∼91%). The red shift can be explained by the coordination of acetonitrile to AlPor. To examine the quenching mechanism, spectral overlap between AlPor fluorescence and H_2Por absorption was estimated (Figure S16a). Significant spectral overlap has been found, although it is slightly smaller compared to the overlap in dichloromethane solution. Despite having a strong spectral overlap, the fluorescence excitation spectrum (collected at 720 nm, Figure 7b) of the dyad did not reveal AlPor excitation bands (at 560 and 610 nm) suggesting that the energy transfer is a minor process or is negligible from the ^{1}AlPor* to H_2Por unit in polar acetonitrile. Hence, the observed strong quenching can be attributed solely to the electron transfer process from ^{1}AlPor* to the H_2Por unit. The Gibbs free energy change (ΔG_{CS}) for this process was found to be −0.54 eV. Furthermore, excitation of the dyad at 640 nm (where 60% light is absorbed by H_2Por) also resulted in quantitative quenching of the 720 nm band, which is exclusively coming from H_2Por (Figure S16b). A careful examination of the energy level diagram suggests that this quenching could be attributed to the electron transfer from AlPor to $^1H_2$Por*, and the corresponding ΔG_{CS} was found to be exergonic by −0.39 eV.

Figure 4b shows the fluorescence spectra of the AlPor-Ph-H_2Por dyad with increasing amounts of pyridine-appended tetrathiafulvalene (TTF-py) in dichloromethane. The excitation wavelength was adjusted to the isosbestic point at 555 nm (where 95% of absorption is due to AlPor). In the absence of TTF-py, the AlPor-Ph-H_2Por dyad shows AlPor bands (I and II) and H_2Por bands (II and III) similar to those of its monomeric compounds AlPor-Ph and H_2Por-Ph. However, their intensities were strongly quenched due to the energy transfer from ^{1}AlPor* to axial H_2Por. Upon addition of TTF-py, the fluorescence bands of AlPor (I and II) shifted to longer wavelengths, and the relative fluorescence intensities of all three bands (I, II and III) are strongly quenched. These notable spectral changes indicate the formation of the TTF-py→AlPor-Ph-H_2Por triad in the solution. However, to explain the possible quenching mechanism/s various control titrations were carried out. Upon addition of py (without the appended TTF unit (Figure S10b)) or TTF (without the appended py group (Figure S9b)) to the dyad, no considerable change in fluorescence intensity was revealed. However, addition of TTF-py to the reference monomer AlPor-Ph revealed an electron transfer process from TTF to the ^{1}AlPor* unit; these results have been reported previously.[42,45] Therefore, the most likely explanation for the quenching of fluorescence bands (I and II) is the electron transfer from TTF to ^{1}AlPor* upon triad formation. This process is exergonic (−0.59 eV) and has been observed in other systems in which TTF was attached axially to a porphyrin macrocycle.[42,45,70,74] Insertion of an additional phenyl spacer between the TTF and py units is expected to decrease the electronic coupling and to slow down the electron

DOI: 10.1021/acs.inorgchem.5b01190
Inorg. Chem. 2015, 54, 8482−8494

transfer rate. Consistent with this expectation, bands I and II are weakly quenched in titrations of TTF-Ph-py vs AlPor-Ph-H_2Por (see Figure S8b), that is, the formation of the TTF-Ph-py→AlPor-Ph-H_2Por triad. Regardless of the fluorescence trends in bands I and II, intriguingly, band III was quenched in both the triads upon addition of py appended TTF derivatives. This could be due to newly introduced electron transfer process between the TTF and ^{1}AlPor* units. As a consequence of the electron transfer, the ^{1}AlPor* state is being quenched rapidly by the TTF unit; hence, the energy transfer from ^{1}AlPor* to H_2Por is expected to be blocked. Thus, band III, which is predominantly the result of the energy transfer process in triads (TTF-py→AlPor-Ph-H_2Por and TTF-Ph-py→AlPor-Ph-H_2Por), reduces significantly. To verify this scheme, the fluorescence excitation spectrum was collected for the triads, TTF-py→AlPor-Ph-H_2Por (Figure 8) and TTF-Ph-py→AlPor-Ph-H_2Por (Figure S17), at 720 nm where the emission is exclusively from the H_2Por unit. As shown in Figure 8, the solid curve represents the absorption spectra of the triad consisting of pyridine coordinated hexavalent AlPor bands (560 and 614 nm) and H_2Por bands (590 and 640 nm) as well as a minor uncomplexed pentavalent AlPor (550 nm). Interestingly, the bands at 560 and 614 nm are completely absent in the excitation spectra (dashed line). These results evidently suggest that the energy transfer is not participating in the quenching of the ^{1}AlPor* state in the triad molecule. Overall, two changes occur in the ^{1}AlPor* state due to the presence of the TTF redox center: (1) it initiates the electron transfer from TTF to ^{1}AlPor*, and (2) it inhibits the energy transfer from ^{1}AlPor* to H_2Por. Moreover, these results suggest that the electron transfer from TTF to ^{1}AlPor* is presumably faster than that of the energy transfer from ^{1}AlPor* to H_2Por.

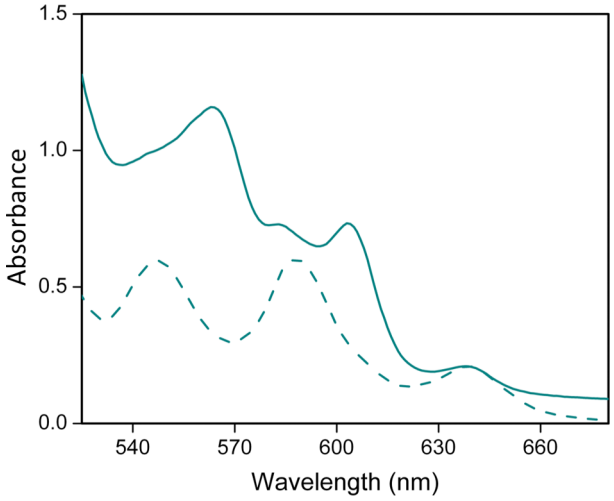

Figure 8. Absorption (solid) and corrected fluorescence excitation (dashed) spectra of the triad TTF-py→AlPor-Ph-H_2Por in dichloromethane. The spectra were normalized between 610 and 650 nm. The excitation spectrum was collected at 720 nm corresponding to the emission of H_2Por. TTF-py and AlPor-Ph-H_2Por are present in 1.88 × 10^{-3} M and 6 × 10^{-5} M in solution, respectively.

Femtosecond Laser Flash Photolysis. Femtosecond transient absorption studies were performed in 1,2-dichlorobenzene (*o*-DCB) (instead of low boiling dichloroemethane) and acetonitrile to secure the evidence of energy transfer, electron transfer, and electron shift processes in the dyad and triads. Samples were excited using 400 nm wavelength light where the absorbance ratio of AlPor and H_2Por is approximately 1:2.

(a). In o-Dichlorobenzene. First, transient spectra of the precursor compounds, AlPor-Ph and H_2Por-Ph, were investigated. As shown in Figure S18a, excitation of AlPor-Ph instantly populated the S_1 and S_2 states with a maximum in the ~450 nm region. At the higher wavelength region, a depleted signal in the Q-band region of AlPor (550 nm), an opposite mimic of the ground state absorption of the Q-band, was observed. In addition, depleted bands at 592 and 648 nm, corresponding to the stimulated emission of Al porphyrin, were observed. Positive peak maxima at 450, 576, 614, and 681 nm were also observed. Interestingly, in the near-IR region, an additional peak at 1256 nm was observed. The decay rate of this peak lasted over 3 ns (see Figure S18b), the monitoring window of our instrument setup, suggesting that this could be due to the singlet−singlet excited state of AlPor.[42] Similarly, the instantly formed S_1 and S_2 states of H_2Por-Ph upon excitation revealed depleted peaks at 509, 533, and 585 nm corresponding to their Q-band absorption, and at 647 and 720 nm corresponding to stimulated emission of free-base porphyrin (Figure S19a). Positive peaks at 440, 530, 558, 616, and 680 nm were observed. In the near-infrared region, a peak at 1067 nm was also observed corresponding to the singlet excited state of free-base porphyrin. The excited singlet state lifetime (τ_S) of

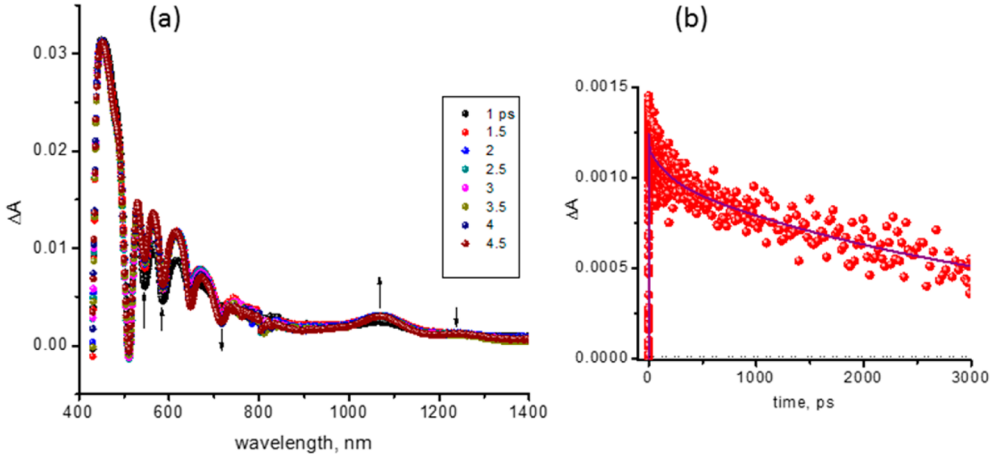

Figure 9. (a) Femtosecond transient absorption spectra and (b) decay profile at 1240 nm of AlPor-Ph-H_2Por in *o*-DCB.

DOI: 10.1021/acs.inorgchem.5b01190
Inorg. Chem. 2015, 54, 8482−8494

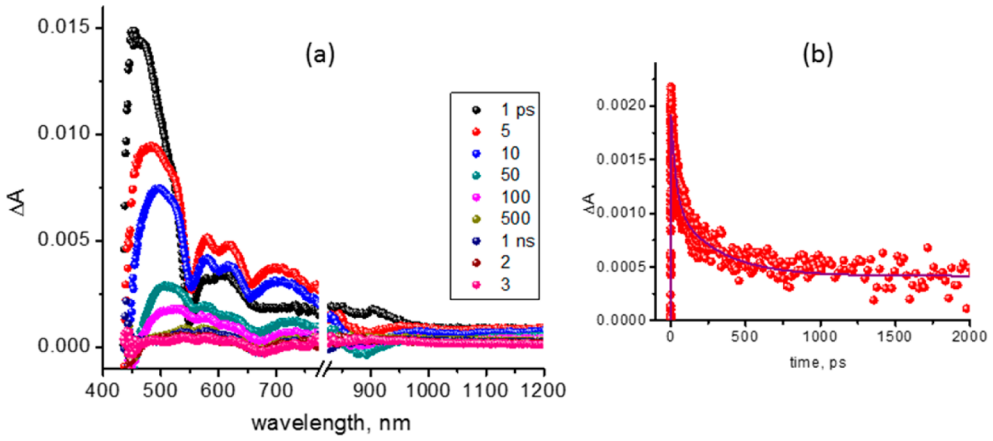

Figure 10. (a) Femtosecond transient absorption spectra and (b) decay profile at 1240 nm of TTF-py→AlPor-Ph (1:3 ratio) in *o*-DCB.

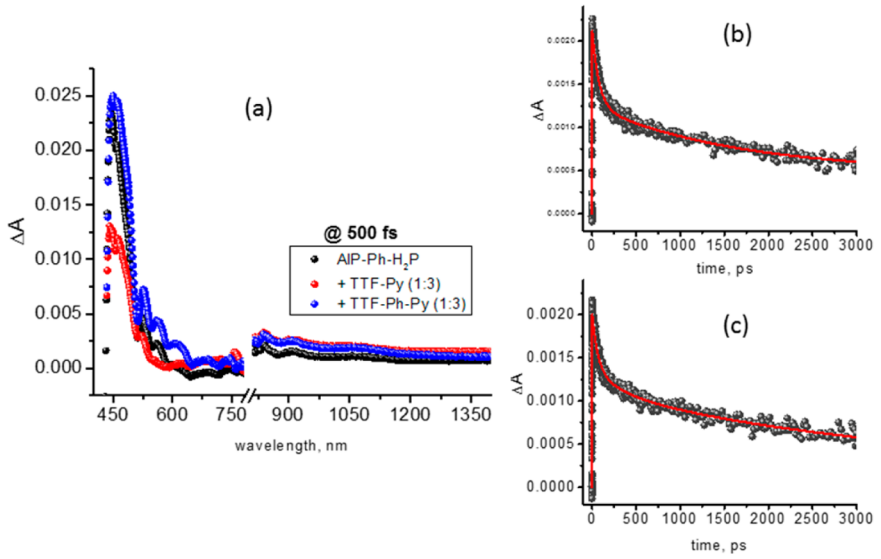

Figure 11. Femtosecond transient absorption spectra of (a) AlPor-Ph-H_2Por (black), TTF-py→AlPor-Ph-H_2Por (red), and TTF-Ph-py→AlPor-Ph-H_2Por (blue) at a delay time of 500 ps, (b) decay profile at 1244 nm of TTF-py→AlPor-Ph-H_2Por, and (c) decay profile at 1244 nm of TTF-Ph-py→AlPor-Ph-H_2Por in *o*-DCB.

AlPor and H_2Por is measured using the time-resolved fluorescence method and found to be 5.80 and 9.00 ns, respectively (see Figure S20 for decay curves) in dichloromethane.

To help interpret the transient spectral data of charge separation products, spectroelectrochemical studies were performed on H_2Por, AlPor, and TTF (Figures S21−S23). The one-electron reduced product of H_2Por-Ph (Figure S21) revealed radical anion peaks at 443, 557, 588, and 632 nm. The Soret band of H_2Por located at 415 nm revealed a red-shift of 28 nm and appeared at 443 nm. The one-electron oxidized product of AlPor-Ph (Figure S22, top spectra) showed peaks at 447, 600, and 685 nm along with broad peaks at 791 and 882 nm. The radical anion of AlPor-Ph (Figure S22, bottom spectra) exhibited peaks at 432, 570, 610, and 645 nm. The Soret band red-shifted from 418 to 432 nm. The radical cation peaks of TTF were located at 450 and 610 nm (Figure S23).

As shown in Figure 9a, femtosecond transient spectra obtained for the AlPor-Ph-H_2Por dyad were rather complex, revealing peaks corresponding to both AlPor and H_2Por entities. That is, negative peaks at 509, 545, 645, and 716, and positive peaks at 448, 528, 565, 618, 671, 1064, and 1240 nm were observed. However, it was possible to secure evidence for singlet−singlet energy transfer from AlPor to H_2Por. At the early time scale, the depleted peaks of AlPor located at 545 and 585 nm recovered faster than that observed for pristine AlPor, while the negative growth of stimulated emission of H_2Por at 646 and 716 nm was much faster than that seen in pristine H_2Por. This was also the case for the singlet peaks of H_2Por at 1064 nm and AlPor at 1240 nm; the former grew in intensity at the expense of the latter. By taking the lifetime and decay rate constant of the AlPor peak at 1240 nm (3.31 ns, 3.02×10^8 s^{-1}) and using a lifetime and rate constant of ^{1}AlPor* (5.80 ns, 1.72×10^8 s^{-1}), a rate constant for energy transfer process, k_{EnT}, in this dyad was estimated to be 1.78×10^8 s^{-1}. As predicted, the coordination of py to AlPor-Ph-H_2Por (which forms a hexavalent Al center) had no noticeable changes in its spectral features (Figure S24).

From steady-state experiments, it was postulated that quenching of the ^{1}AlPor* state in the dyads TTF-Ph_n-py→AlPor-Ph (n = 0, 1) is due to the electron transfer from TTF to the ^{1}AlPor* unit. To verify this claim, femtosecond transient absorption studies were performed on these dyads. As shown in Figure 10a, upon excitation of the dyad (TTF-py→AlPor-Ph),

DOI: 10.1021/acs.inorgchem.5b01190
Inorg. Chem. 2015, 54, 8482−8494

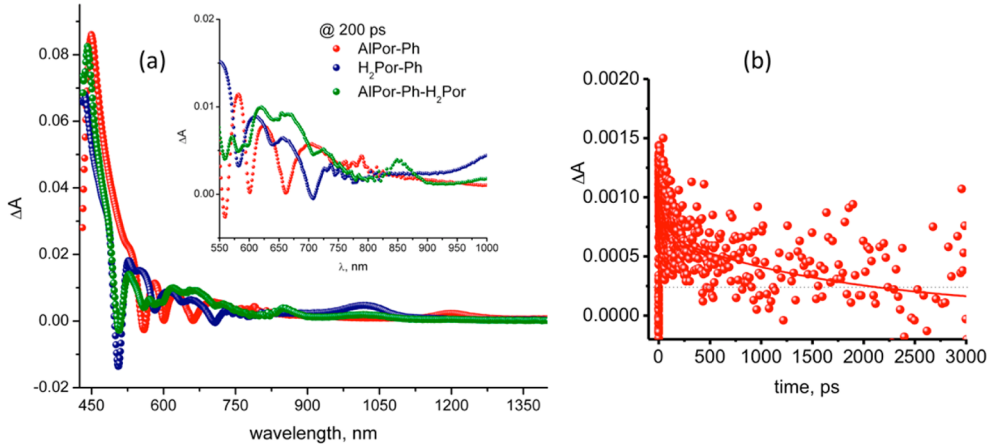

Figure 12. (a) Femtosecond transient absorption spectra of AlPor-Ph (red), H_2Por-Ph (blue), and AlPor-Ph-H_2Por (green) at 200 ps, and (b) time profile at ~1205 nm of AlPor-Ph-H_2Por in acetonitrile.

absorbance with a maximum in the ~450 nm region characteristic of the ^{1}AlPor* state was observed. Subsequently, the ^{1}AlPor* state evolved into the TTF$^{+\bullet}$AlPor$^{-\bullet}$ charge-separated state with a rate constant (k_{ET}) of 1.25 × 10^{10} s^{-1} (see Figure 10b). This state can be readily identified by distinctive peaks for TTF$^{+\bullet}$ in the ~496 nm region, and at ~570 and ~610 nm for the counterpart AlPor$^{-\bullet}$. Similarly, the transient absorption spectra of the TTF-Ph-py→AlPor-Ph dyad was measured, and the spectra are shown in Figure S25. As anticipated, the charge-separated state TTF$^{+\bullet}$AlPor$^{-\bullet}$ formed with a rate constant of 8.33 × 10^9 s^{-1}, which is slightly slower than the rate constant in TTF-py→AlPor-Ph. This is because of the increased distance between TTF and AlPor in TTF-Ph-py→AlPor-Ph due to an extra phenyl spacer unit. Overall, these results conclude the occurrence of electron transfer in TTF-Ph$_n$-py→AlPor-Ph (n = 0, 1) dyads that are consistent with steady-state fluorescence results.

For transient absorption studies, triads (TTF-py→AlPor-Ph-H_2Por and TTF-Ph-py→AlPor-Ph-H_2Por) were prepared by adding the TTF-py or TTF-Ph-py (0.15 mM) to AlPor-Ph-H_2Por (0.05 mM) in o-DCB. The resultant solutions were excited at 400 nm where the absorption ratio of AlPor and H_2Por is 1:2. As shown in Figure S26, the transient spectra of the triads appeared to be even more complex, and identifying spectral features was a challenging task. This is because of two reasons: (i) due to the moderate binding constant between TTF-py (or TTF-Ph-py) and AlPor-Ph-H_2Por, the experimental solutions comprised only ~25% (0.013 mM) of the triad and the remaining ~75% of the sample existed as individual components, and (ii) due to the strong spectral presence of AlPor and H_2Por in the monitoring visible region, it was difficult to isolate the TTF$^{+\bullet}$, AlPor$^{-\bullet}$, and H_2Por$^{-\bullet}$ radical ion peaks. However, the early spectral features (<1 ps after excitation) to some extent suggest the occurrence of electron transfer and electron shift processes in the presence of a TTF unit. Figure 11 shows the absorption changes at 500 fs after excitation of the sample. There are significant differences in spectral features of the dyad and its corresponding triads. The absorbance change (ΔA) diminished to half for the TTF-py→AlPor-Ph-H_2Por triad compared to its reference dyad (AlPor-Ph-H_2Por) suggesting a rapid quenching of the ^{1}AlPor* state by the electron transfer from the TTF unit. In the case of the TTF-Ph-py→AlPor-Ph-H_2Por triad, the absorbance change was found to be higher than that of the TTF-py→AlPor-Ph-H_2Por triad, which indicates that the electron transfer is slightly slower because of the extra phenyl ring between the TTF and AlPor units. The formation of TTF$^{+\bullet}$ and AlPor$^{-\bullet}$, expected to result in absorption changes in the 450−500 nm and 600−650 nm region, respectively, were also observed, although they were overlapped with other peaks in this wavelength region. After 1 ps, the visible region is obscured by intense spectral features from the dyad (unbound 75%). Hence, it was challenging to track the time course of electron shift and charge recombination processes. However, further evidence for electron transfer came from the near-IR peak of AlPor as it undergoes an additional quenching (Figure 11b and c and Figure 9b). Whereas, evidence for the electron shift from AlPor$^{-\bullet}$ to H_2Por is inferred from the observed low efficiency of energy transfer from ^{1}AlPor* to H_2Por. As shown in Figure S27, the depleted emission of the free-base porphyrin at ~647 nm decreases, which suggest the ^{1}AlPor* state is involved in the electron transfer process rather than energy transfer in the triad (TTF-py→AlPor-Ph-H_2Por or TTF-Ph-py→AlPor-Ph-H_2Por) molecule.

(b). In Acetonitrile. To establish evidence for charge-separation in polar solvents, femtosecond transient absorption studies were performed on the dyad (AlPor-Ph-H_2Por) and its reference monomers (AlPor-Ph and H_2Por-Ph) in acetonitrile. As shown in Figure S28a, for AlPor-Ph there were instantly populated S_1 and S_2 states, bleaching due to both absorption (558 nm) and emission (598 and 660 nm) peaks, and positive peak maxima (450, 580, 627, and 704 nm), and a near-infrared (1205 nm) peak was observed. The other reference compound, H_2Por-Ph (Figure S29a), showed instantaneous formation of the S_1 and S_2 states, bleaching due to the absorption (505, 539, and 581 nm), and stimulated emission (635 and 707 nm) peaks, positive peaks (440, 530, 558, 616, and 680 nm), and also the near-infrared (1023 nm) peak. The observed near-infrared peaks for AlPor-Ph and H_2Por-Ph correspond to singlet−singlet transition, and they decayed slower than the 3 ns monitoring window of our instrument setup (Figures S28b and S29b). Figure 12 shows the femtosecond transient absorption spectra of AlPor-Ph-H_2Por in acetonitrile at 200 ps (see Figure S30 for spectra at other delay times). The spectra revealed peaks from both the AlPor and H_2Por units. However, the observed peaks decayed rapidly, while the bleaching at 505 and 558 nm was recovered faster than their pristine compounds. The formation of AlPor$^{+\bullet}$ and H_2Por$^{-\bullet}$,

DOI: 10.1021/acs.inorgchem.5b01190
Inorg. Chem. 2015, 54, 8482−8494

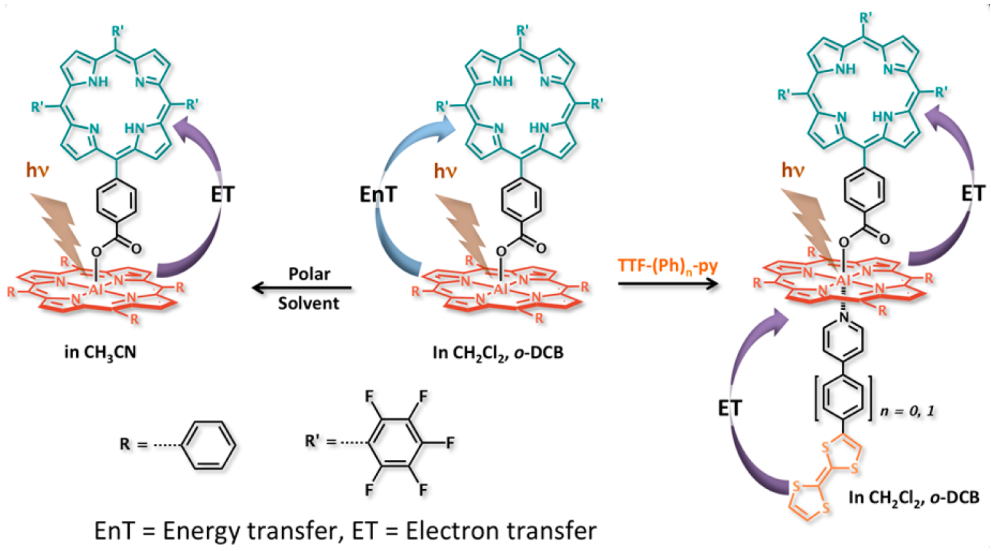

Figure 13. Proposed modulation of photoinduced processes in the dyad and its corresponding triads.

anticipated to result in absorption changes in the 540−590 nm and 600−650 nm region, respectively, was also observed (Figure 12a, inset). By monitoring the near-infrared peak of AlPor, the rate of charge separation was estimated to be 1.79×10^8 s^{-1} (Figures 12b). Transient absorption studies on triad solutions were not carried out because the experimental solutions contain a very small amount of the triad molecule. These lower concentrations are caused by the competition between TTF-Ph_n-py and CH_3CN binding to the Al center.

Modulation of Energy Transfer into Electron Transfer. Figure 13 summarizes the photoinduced processes that are involved in the dyad and its corresponding triads. Upon photoexcitation of AlPor in the dyad in noncoordinating solvents (dichloromethane or *o*-DCB), the AlPor moiety serves as an antenna by transferring its singlet excitation to the H_2Por with a rate constant (k_{EnT}) of 1.78×10^8 s^{-1}. In contrast, the same AlPor in the dyad acts as an electron acceptor in the presence of TTF (i.e., formation of triad) and it initiates a sequential electron transfer between TTF, AlPor, and H_2Por components. In triads, photoexcitation of the AlPor results in rapid electron transfer from TTF to ^{1}AlPor* with a rate constant (k_{ET}) of $8.33 \times 10^9 - 1.25 \times 10^{10}$ s^{-1} to yield a primary radial pair $TTF^{+\bullet}$-$AlPor^{-\bullet}$-H_2Por. This is followed by an electron shift to produce the final charge separated state $TTF^{+\bullet}$-AlPor-$H_2Por^{-\bullet}$. The electron transfer between TTF and ^{1}AlPor* redox centers was found to be nearly two orders of magnitude faster than the energy transfer between ^{1}AlPor* and H_2Por entities. Consequently, the electron transfer outperforms the energy transfer process and generates the primary radical ion-pair, which ultimately undergoes an electron shift to yield the final radical ion-pair. Therefore, these results represent the modulation of energy transfer into sequential electron transfer via axial coordination of the TTF moiety.

As revealed by transient spectral studies, energy transfer is the main quenching mechanism for ^{1}AlPor* in the dyad and AlPor-Ph-H_2Por in nonpolar solvents. However, this is no longer the case in the triads (TTF-Ph_n-py→AlPor-Ph-H_2Por, n = 0,1) where a new decay pathway for the ^{1}AlPor* state opens up in the presence of the electron rich TTF moiety. The optical studies identified electron transfer as the new process from TTF to ^{1}AlPor*, and moreover, it was found to be much faster than the energy transfer from ^{1}AlPor* to H_2Por. These results can be explained by using the electronic coupling between TTF and AlPor units as well as the Gibbs free energy change. Our recent DFT studies on TTF-Ph_n-py→AlPor-Ph (n = 0,1), where the py appended TTF derivatives were bound to pristine AlPor-Ph through a coordination bond in the axial direction, revealed a significant delocalization of their molecular orbitals (HOMO and LUMO) onto the bridging unit.[42,45] As anticipated, the HOMO and LUMO are localized primarily on the TTF and AlPor units, respectively. However, in both cases some delocalization onto the Ph and/or Py bridge occurs. This results in a substantial electronic coupling between donor (TTF) and acceptor (AlPor) units, which could potentially favor the electron transfer process. Furthermore, Figure 5 reveals that the electron transfer process is more exergonic (−0.59 eV) than the energy transfer (−0.15 eV) process. Together with strong electronic coupling and large driving force, it is reasonable to expect that the ^{1}AlPor* state in the triad would quench strongly by rapid electron transfer rather than energy transfer.

CONCLUSIONS

The above presented results show that it is possible to construct multicomponent "donor-AlPor-acceptor" systems in the axial direction by exploiting the unique properties of AlPor. Excited state properties revealed that energy transfer (major) and electron transfer (minor) from ^{1}AlPor* to H_2Por coexist in the dyad (AlPor-Ph-H_2Por) molecule. However, the relative ratio can be modulated (i) by changing the solvent polarity or (ii) by converting the dyad (AlPor-Ph-H_2Por) into a triad (TTF-Ph_n-py→AlPor-Ph-H_2Por, n = 0,1) using the secondary electron donor (TTF) through axial linkage. These results represent the first such example where the energy donor is converted into an electron acceptor/donor through axial coordination of the TTF moiety. However, the pyridine unit was found to be less optimal for linking the TTF to the dyad molecules. Because of its moderate binding constant, the equilibrium in triad solutions always pushed more toward the dyad in our experimental solutions (Figure 1). This hampered the tracking of electron shift and charge recombination processes in the triad molecule. Recent studies suggest that

DOI: 10.1021/acs.inorgchem.5b01190
Inorg. Chem. 2015, 54, 8482−8494

imidazole binds two orders of magnitude stronger than pyridine.[47] Currently, we are exploring these ideas in the construction of new triads with a better association constant.

■ ASSOCIATED CONTENT

Supporting Information

The Supporting Information is available free of charge on the ACS Publications website at DOI: 10.1021/acs.inorgchem.5b01190.

Synthesis details, NMR, and absorption spectra, titrations (absorption and florescence), binding constants, estimation of E_{0-0} energies, cyclic voltammetry, phosphorescence spectra, steady-state optical data (spectral overlap, fluorescence spectra, and excitation spectra), spectroelectrochemistry, and transient absorption spectra (PDF)

■ AUTHOR INFORMATION

Corresponding Authors

*(P.K.P.) E-mail: ppoddutoori@upei.ca.

*(F.D.) E-mail: Francis.DSouza@unt.edu.

Notes

The authors declare no competing financial interest.

■ ACKNOWLEDGMENTS

This work was supported by the Department of Chemistry, University of Prince Edward Island, Canada and the US-National Science Foundation (Grant No. 1401188 to F.D.). R.K. acknowledges financial support from the Natural Sciences and Engineering Research Council (NSERC) and the Canada Foundation for Innovation (CFI). Also, we thank Professor Art van der Est and Professor Melanie Pilkington (Department of Chemistry, Brock University) for providing resources for the synthesis of TTF derivatives. Dr. Serguei Vassiliev is thanked for the time-resolved fluorescence studies.

■ REFERENCES

(1) Yang, J.; Yoon, M. C.; Yoo, H.; Kim, P.; Kim, D. *Chem. Soc. Rev.* **2012**, *41*, 4808.

(2) Aratani, N.; Kim, D.; Osuka, A. *Acc. Chem. Res.* **2009**, *42*, 1922.

(3) Choi, M. S.; Yamazaki, T.; Yamazaki, I.; Aida, T. *Angew. Chem., Int. Ed.* **2004**, *43*, 150.

(4) Van Patten, P. G.; Shreve, A. P.; Lindsey, J. S.; Donohoe, R. J. *J. Phys. Chem. B* **1998**, *102*, 4209.

(5) Imahori, H. *J. Phys. Chem. B* **2004**, *108*, 6130.

(6) Wasielewski, M. R. *Chem. Rev.* **1992**, *92*, 435.

(7) Liu, J. Y.; El-Khouly, M. E.; Fukuzumi, S.; Ng, D. K. P. *Chem. - Eur. J.* **2011**, *17*, 1605.

(8) Guldi, D. M. *Chem. Soc. Rev.* **2002**, *31*, 22.

(9) D'Souza, F.; Gadde, S.; Islam, D. M. S.; Wijesinghe, C. A.; Schumacher, A. L.; Zandler, M. E.; Araki, Y.; Ito, O. *J. Phys. Chem. A* **2007**, *111*, 8552.

(10) Wasielewski, M. R. *J. Org. Chem.* **2006**, *71*, 5051.

(11) Wasielewski, M. R. *Acc. Chem. Res.* **2009**, *42*, 1910.

(12) Maligaspe, E.; Tkachenko, N. V.; Subbaiyan, N. K.; Chitta, R.; Zandler, M. E.; Lemmetyinen, H.; D'Souza, F. *J. Phys. Chem. A* **2009**, *113*, 8478.

(13) Luo, C.; Guldi, D. M.; Imahori, H.; Tamaki, K.; Sakata, K. *J. Am. Chem. Soc.* **2000**, *122*, 6535.

(14) Liddell, P. A.; Kodis, G.; de la Garza, L.; Moore, A. L.; Moore, T. A.; Gust, D. *J. Phys. Chem. B* **2004**, *108*, 10256.

(15) Kodis, G.; Terazono, Y.; Liddell, P. A.; Andreasson, J.; Garg, V.; Hambourger, M.; Moore, T. A.; Moore, A. L.; Gust, D. *J. Am. Chem. Soc.* **2006**, *128*, 1818.

(16) Kobuke, Y.; Ogawa, K. *Bull. Chem. Soc. Jpn.* **2003**, *76*, 689.

(17) Imahori, H.; Mori, Y.; Matano, Y. *J. Photochem. Photobiol., C* **2003**, *4*, 51.

(18) Gust, D.; Moore, T. A.; Moore, A. L. *Acc. Chem. Res.* **2009**, *42*, 1890.

(19) Fukuzumi, S. *Phys. Chem. Chem. Phys.* **2008**, *10*, 2283.

(20) Holten, D.; Bocian, D. F.; Lindsey, J. S. *Acc. Chem. Res.* **2002**, *35*, 57.

(21) Raymo, F. M.; Tomasulo, M. *Chem. Soc. Rev.* **2005**, *34*, 327.

(22) *Handbook of Porphyrin Science*; Kadish, K. M., Smith, K. M., Guilard, R., Eds.; World Scientific: Singapore, 2010.

(23) Ward, M. D. *Chem. Soc. Rev.* **1997**, *26*, 365.

(24) Hayashi, T.; Ogoshi, H. *Chem. Soc. Rev.* **1997**, *26*, 355.

(25) Liddell, P. A.; Kodis, G.; de la Garza, L.; Bahr, J. L.; Moore, A. L.; Moore, T. A.; Gust, D. *Helv. Chim. Acta* **2001**, *84*, 2765.

(26) D'Souza, F.; Ito, O. *Chem. Commun.* **2009**, 4913.

(27) Gust, D.; Moore, T. A. *Top. Curr. Chem.* **1991**, *159*, 103.

(28) Gust, D.; Moore, T. A.; Moore, A. L. *Acc. Chem. Res.* **1993**, *26*, 198.

(29) Wilson, S. R.; MacMahon, S.; Tat, F. T.; Jarowski, P. D.; Schuster, D. I. *Chem. Commun.* **2003**, 226.

(30) Trabolsi, A.; Elhabiri, M.; Urbani, M.; de la Cruz, J. L. D.; Ajamaa, F.; Solladie, N.; Albrecht-Gary, A. M.; Nierengarten, J. F. *Chem. Commun.* **2005**, 5736.

(31) Stangel, C.; Schubert, C.; Kuhri, S.; Rotas, G.; Margraf, J. T.; Regulska, E.; Clark, T.; Torres, T.; Tagmatarchis, N.; Coutsolelos, A. G.; Guldi, D. M. *Nanoscale* **2015**, *7*, 2597.

(32) Schuster, D. I.; Cheng, P.; Jarowski, P. D.; Guldi, D. M.; Luo, C. P.; Echegoyen, L.; Pyo, S.; Holzwarth, A. R.; Braslavsky, S. E.; Williams, R. M.; Klihm, G. *J. Am. Chem. Soc.* **2004**, *126*, 7257.

(33) Kim, H. J.; Park, K. M.; Ahn, T. K.; Kim, S. K.; Kim, K. S.; Kim, D. H.; Kim, H. J. *Chem. Commun.* **2004**, 2594.

(34) Fukuzumi, S.; Honda, T.; Ohkubo, K.; Kojima, T. *Dalton Trans.* **2009**, 3880.

(35) Fazio, M. A.; Durandin, A.; Tkachenko, N. V.; Niemi, M.; Lemmetyinen, H.; Schuster, D. I. *Chem. - Eur. J.* **2009**, *15*, 7698.

(36) D'Souza, F.; Maligaspe, E.; Karr, P. A.; Schumacher, A. L.; El Ojaimi, M.; Gros, C. P.; Barbe, J. M.; Ohkubo, K.; Fukuzumi, S. *Chem.—Eur. J.* **2008**, *14*, 674.

(37) El-Khouly, M. E.; Ito, O.; Smith, P. M.; D'Souza, F. *J. Photochem. Photobiol., C* **2004**, *5*, 79.

(38) Lazarides, T.; Kuhri, S.; Charalambidis, G.; Panda, M. K.; Guldi, D. M.; Coutsolelos, A. G. *Inorg. Chem.* **2012**, *51*, 4193.

(39) Panda, M. K.; Lazarides, T.; Charalambidis, G.; Nikolaou, V.; Coutsolelos, A. G. *Eur. J. Inorg. Chem.* **2015**, *2015*, 468.

(40) Shetti, V. S.; Ravikanth, M. *Inorg. Chem.* **2011**, *50*, 1713.

(41) Xu, H.; Ng, D. K. P. *Inorg. Chem.* **2008**, *47*, 7921.

(42) Poddutoori, P. K.; Lim, G. N.; Sandanayaka, A. S. D.; Karr, P. A.; Ito, O.; D'Souza, F.; Pilkington, M.; van der Est, A. *Nanoscale* **2015**, *7*, 12151.

(43) Poddutoori, P. K.; Sandanayaka, A. S. D.; Hasobe, T.; Ito, O.; van der Est, A. *J. Phys. Chem. B* **2010**, *114*, 14348.

(44) Poddutoori, P. K.; Sandanayaka, A. S. D.; Zarrabi, N.; Hasobe, T.; Ito, O.; van der Est, A. *J. Phys. Chem. A* **2011**, *115*, 709.

(45) Poddutoori, P. K.; Zarrabi, N.; Moiseev, A. G.; Gumbau-Brisa, R.; Vassiliev, S.; van der Est, A. *Chem. - Eur. J.* **2013**, *19*, 3148.

(46) Metselaar, G. A.; Sanders, J. K. M.; de Mendoza, J. *Dalton Trans.* **2008**, 588.

(47) Davidson, G. J. E.; Tong, L. H.; Raithby, P. R.; Sanders, J. K. M. *Chem. Commun.* **2006**, 3087.

(48) Iengo, E.; Cavigli, P.; Gamberoni, M.; Indelli, M. T. *Eur. J. Inorg. Chem.* **2014**, *2014*, 337.

(49) Iengo, E.; Pantos, G. D.; Sanders, J. K. M.; Orlandi, M.; Chiorboli, C.; Fracasso, S.; Scandola, F. *Chem. Sci.* **2011**, *2*, 676.

(50) Poddutoori, P. K.; Poddutoori, P.; Maiya, B. G.; Prasad, T. K.; Kandrashkin, Y. E.; Vasil'ev, S.; Bruce, D.; van der Est, A. *Inorg. Chem.* **2008**, *47*, 7512.

(51) Prashanth Kumar, P.; Maiya, B. G. *New J. Chem.* **2003**, *27*, 619.

DOI: 10.1021/acs.inorgchem.5b01190
Inorg. Chem. 2015, 54, 8482−8494

(52) Ghosh, A.; Maity, D. K.; Ravikanth, M. *New J. Chem.* **2012**, *36*, 2630.
(53) Natali, M.; Argazzi, R.; Chiorboli, C.; Iengo, E.; Scandola, F. *Chem. - Eur. J.* **2013**, *19*, 9261.
(54) Hirai, Y.; Aida, T.; Inoue, S. *J. Am. Chem. Soc.* **1989**, *111*, 3062.
(55) Davidson, G. J. E.; Lane, L. A.; Raithby, P. R.; Warren, J. E.; Robinson, C. V.; Sanders, J. K. M. *Inorg. Chem.* **2008**, *47*, 8721.
(56) van der Est, A.; Poddutoori, P. *Appl. Magn. Reson.* **2013**, *44*, 301.
(57) Kanematsu, M.; Naumov, P.; Kojima, T.; Fukuzumi, S. *Chem. - Eur. J.* **2011**, *17*, 12372.
(58) *The Photosynthetic Reaction Center*; Deisenhofer, J., Norris, J. R., Eds.; Academic Press: San Diego, CA, 1993.
(59) Deisenhofer, J.; Epp, O.; Miki, K.; Huber, R.; Michel, H. *J. Mol. Biol.* **1984**, *180*, 385.
(60) Barber, J.; Andersson, B. *Nature* **1994**, *370*, 31.
(61) Fromme, P. *Curr. Opin. Struct. Biol.* **1996**, *6*, 473.
(62) Krauss, N.; Schubert, W. D.; Klukas, O.; Fromme, P.; Witt, H. T.; Saenger, W. *Nat. Struct. Biol.* **1996**, *3*, 965.
(63) Huber, R. *Angew. Chem., Int. Ed. Engl.* **1989**, *28*, 848.
(64) Deisenhofer, J.; Michel, H. *Angew. Chem., Int. Ed. Engl.* **1989**, *28*, 829.
(65) Di Valentin, M.; Bisol, A.; Agostini, G.; Liddell, P. A.; Kodis, G.; Moore, A. L.; Moore, T. A.; Gust, D.; Carbonera, D. *J. Phys. Chem. B* **2005**, *109*, 14401.
(66) Kodis, G.; Liddell, P. A.; de la Garza, L.; Moore, A. L.; Moore, T. A.; Gust, D. *J. Mater. Chem.* **2002**, *12*, 2100.
(67) Gust, D.; Moore, T. A.; Moore, A. L.; Leggett, L.; Lin, S.; Degraziano, J. M.; Hermant, R. M.; Nicodem, D.; Craig, P.; Seely, G. R.; Nieman, R. A. *J. Phys. Chem.* **1993**, *97*, 7926.
(68) Gust, D.; Moore, T. A.; Moore, A. L.; Gao, F.; Luttrull, D.; Degraziano, J. M.; Ma, X. C. C.; Makings, L. R.; Lee, S. J.; Trier, T. T.; Bittersmann, E.; Seely, G. R.; Woodward, S.; Bensasson, R. V.; Rougee, M.; Deschryver, F. C.; Vanderauweraer, M. *J. Am. Chem. Soc.* **1991**, *113*, 3638.
(69) Benesi, H. A.; Hildebrand, J. H. *J. Am. Chem. Soc.* **1949**, *71*, 2703.
(70) Poddutoori, P. K.; Dion, A.; Yang, S. J.; Pilkington, M.; Wallis, J. D.; van der Est, A. *J. Porphyrins Phthalocyanines* **2010**, *14*, 178.
(71) Rehm, D.; Weller, A. *Berichte Der Bunsen-Gesellschaft Fur Physikalische Chemie* **1969**, *73*, 834.
(72) Rehm, D.; Weller, A. *Isr. J. Chem.* **1970**, *8*, 259.
(73) The structures were optimized by using Avogadro 1.1.1. de Jong, W. A.; Walker, A. M.; Hanwell, M. D. *J. Cheminformatics* **2013**, *5*. The radii of AlPor and TTF were found to be within ± 0.1 Å compared to the values that were obtained from the DFT calcuations; see ref 42. Therefore, it is reasonable to use these values (R_{AlPor} = 7.77 Å, R_{H2Por} = 7.81 Å, and R_{TTF} = 5.55 Å) in the calculations of G_S. Also, the center-to-center distances in AlPor-Ph-H_2Por, TTF-py→AlPor-Ph-H_2Por, and TTF-Ph-py→AlPor-Ph-H_2Por were estimated to be 11.83 Å, 21.38 Å, and 25.43 Å, respectively.
(74) Xiao, X. W.; Xu, W.; Zhang, D. Q.; Xu, H.; Lu, H. Y.; Zhu, D. B. *J. Mater. Chem.* **2005**, *15*, 2557.

DOI: 10.1021/acs.inorgchem.5b01190
Inorg. Chem. 2015, 54, 8482−8494